2020 IEEE/RSJ International Conference on Intelligent Robots and Systems (IROS)
October 25-29, 2020, Las Vegas, NV, USA (Virtual)

Automatic Targetless Extrinsic Calibration of Multiple 3D LiDARs and Radars

Lionel Heng

Abstract— **Many self-driving vehicles use a multi-sensor system comprising multiple 3D LiDAR and radar sensors for robust all-round perception. Precise calibration of this multi-sensor system is a critical prerequisite for accurate perception data which facilitates safe operation of self-driving vehicles in highly dynamic urban environments. This paper proposes the first-known automatic targetless method for extrinsic calibration of multiple 3D LiDAR and radar sensors, and which only requires the vehicle to be driven over a short distance. The proposed method first estimates the 6-DoF pose of each LiDAR sensor with respect to the vehicle reference frame by minimizing point-to-plane distances between scans from different LiDAR sensors. In turn, a 3D map of the environment is built using data from all calibrated LiDAR sensors on the vehicle. We find the 6-DoF pose of each radar sensor with respect to the vehicle reference frame by minimizing (1) point-to-plane distances between radar scans and the 3D map, and (2) radial velocity errors. Our proposed calibration method does not require overlapping fields of view between LiDAR and radar sensors. Real-world experiments demonstrate the accuracy and repeatability of the proposed calibration method.**

I. INTRODUCTION

LiDARs and radars are popular choices of sensors on self-driving vehicles because of their ability to perceive in 3D and both day and night. Whereas a LiDAR sensor generates a dense point cloud of the environment, a radar sensor generates a very sparse point cloud but with radial velocity information which is beneficial for moving object detection and tracking. In addition, radar sensors are able to see through fog, rain, and snow unlike their LiDAR counterparts, and enable self-driving vehicles to operate safely in adverse weather conditions. With advances in sensor technology, LiDAR and radar sensors are able to capture environmental details at higher resolutions and at longer ranges. In addition, today's radar sensors can record the elevation for each point measurement in addition to range, azimuth, and radial velocity. This recent development in radar sensor technology allows us to register radar scans to LiDAR scans in 3D space, and thus, makes possible 6-DoF extrinsic calibration between multiple 3D LiDAR and radar sensors.

Robust operation of self-driving vehicles in highly dynamic urban environments requires omni-directional sensing. Hence, a self-driving vehicle is typically equipped with both an all-surround multi-LiDAR system and an all-surround multi-radar system. For fusion of sensor data from multiple sensors of the same or different sensing modalities to happen, these multiple sensors have to be calibrated accurately with respect to a common reference frame.

*Lionel Heng is with the Robotics Autonomy Lab, Robotics Division, DSO National Laboratories, Singapore lionel.heng@ieee.org

Target-based calibration methods are often time-consuming and labor-intensive, and require the presence of a calibration target for each round of calibration. In this paper, we propose a fully automatic and targetless calibration method for multiple 3D LiDAR and radar sensors and which allows the vehicle to be calibrated anywhere and anytime. By exploiting the capability of both LiDAR and radar sensors to capture information about the 3D geometry of the environment and using this 3D information for inter-sensor registration, we eliminate the need for a calibration target.

We list the novel contributions of our paper:

1) Our proposed method is the first-known method for automatic targetless extrinsic calibration of multiple 3D LiDAR and radar sensors.
2) For non-linear least-squares optimization in extrinsic multi-radar calibration, we formulate novel residuals which exploit all the properties of radar measurements: range, azimuth, elevation, and radial velocity, allowing us to maximize calibration accuracy and repeatability.

II. RELATED WORK

Automatic targetless methods exist for extrinsic calibration of multiple 3D LiDAR sensors [1], extrinsic calibration of multiple 2D and 3D LiDAR sensors [2], extrinsic calibration of multiple cameras [3], extrinsic calibration of a camera-LiDAR sensor pair [4], and extrinsic calibration of a camera-radar sensor pair [5]. For extrinsic multi-3D-LiDAR calibration, Jiao et al. [1] perform hand-eye calibration to find the initial extrinsic parameters, and refine them through the point-to-plane Iterative Closest Point (ICP) algorithm. It is worth noting that point-to-plane ICP cannot be directly applied to extrinsic multi-radar sensors. Radar range measurements are more sparse and less accurate than LiDAR range measurements by at least an order of magnitude. As a result, plane normals computed from single or accumulated radar scans are inaccurate, and prevent convergence of point-to-plane ICP. Our approach overcomes this issue by using a highly precise 3D map built with 3D LiDAR sensors to calibrate each radar sensor; calibration is based on registration of the radar scans with the 3D map. Maddern et al. [2] find the pose of each 3D LiDAR sensor with respect to the vehicle reference frame by maximizing an entropy-based cost function, subsequently construct a 3D map of the environment from all 3D LiDAR sensors, and find the pose of each 2D LiDAR sensor with respect to the vehicle reference frame by maximizing a cross-entropy-based cost function based on the 3D map. Our calibration method is

similar in spirit; we calibrate each 3D LiDAR sensor to the vehicle reference frame, build a 3D map from all 3D LiDAR sensors, and calibrate each radar sensor to the vehicle reference frame using the 3D map. Heng et al. [3] calibrate a multi-camera system to the vehicle reference frame by running stereo visual odometry for each pair of cameras with overlapping fields of view and minimizing the sum of squared reprojection errors over all feature tracks from stereo visual odometry. Pandey et al. [4] calibrate a camera to a 2D/3D LiDAR sensor by leveraging reflectivity values from LiDAR returns and intensity values from camera images and maximizing a mutual-information-based cost function. Schöller et al. [5] calibrate a camera to a radar sensor by feeding camera images and projected radar detections into a deep network, which in turn, outputs a quaternion representing the relative rotation between the camera and radar sensor. We note that no automatic targetless method exists for extrinsic calibration of multiple 3D LiDAR and radar sensors.

There are existing target-based methods for extrinsic calibration of 3D LiDAR and radar sensors. Peršić et al. [6] use a trihedral corner reflector with a flat styrofoam triangle board in front as a calibration target. The LiDAR scan is segmented into planes, and the plane corresponding to the triangle board corresponds to the 3D position of the calibration target in the LiDAR sensor frame. At the same time, point measurements with high radar-cross-section values and from the radar sensor are selected and averaged to yield the 3D position of the calibration target in the radar sensor frame. The extrinsic calibration parameters are found through minimization of the squared distances between multiple pairs of target position measurements from LiDAR and radar. Domhof et al. [7] employ a similar approach with a calibration target comprising a trihedral corner reflector and a flat styrofoam board with cut-out circles. Our calibration method does away with the need for a calibration target by leveraging information about the 3D geometry of the environment. In addition, as our calibration method exploits a 3D map built from accumulation of 3D LiDAR scans over a short distance to calibrate individual radar sensors, it does not require overlapping fields of view between a 3D LiDAR and a radar sensor.

Izquierdo et al. [8] propose a targetless approach for extrinsic calibration of multiple radar sensors using a high-definition (HD) map storing the positions of objects with specific classes and high radar cross-section: street lights and traffic signs. They assume that the vehicle is able to localize in the HD map with less than 2 cm accuracy using RTK GNSS, and register the radar scans to the calibration targets to obtain the extrinsic calibration. Our calibration method avoids the need for high-precision localization and a HD map by building a local HD map with 3D LiDAR sensors on the fly.

Kellner et al. [9] find the rotation of a radar sensor with respect to the vehicle reference frame; the translation is known beforehand from a CAD model. They estimate the linear velocity of the radar sensor from stationary point measurements by minimizing the errors between the measured and expected radial velocities, and in turn, estimate the relative rotation between the radar and vehicle reference frames by comparing lateral velocity measurements from a gyroscope to the lateral velocity estimates for the radar sensor. In contrast, our calibration method is able to recover the full 6-DoF pose of each radar sensor with respect to the vehicle reference frame. Instead of indirectly using radial velocity measurements for the estimation of the radar sensor pose, we find the radar sensor pose by directly minimizing the errors between the measured and expected radial velocities in addition to point-to-plane distances between the radar scans and a 3D map.

III. Notation

We briefly define the notation to be used throughout this paper. We denote the world reference frame as $\underrightarrow{\mathcal{F}}_W$, the vehicle reference frame as $\underrightarrow{\mathcal{F}}_V$, and the sensor reference frame as $\underrightarrow{\mathcal{F}}_S$.

We denote the sensor pose with respect to $\underrightarrow{\mathcal{F}}_V$ as a rigid body transformation $\mathbf{T}_{VS} \in SE(3)$ from $\underrightarrow{\mathcal{F}}_S$ to $\underrightarrow{\mathcal{F}}_V$ and whose rotation matrix part is $\mathbf{R}_{VS}$ and translation part is $\mathbf{t}_{VS}$. Likewise, we denote the sensor pose in $\underrightarrow{\mathcal{F}}_W$ as $\mathbf{T}_{WS} = \mathbf{T}_{WV}\,\mathbf{T}_{VS}$ where $\mathbf{T}_{WV}$ is the vehicle pose in $\underrightarrow{\mathcal{F}}_W$ and can be obtained from a GNSS/INS system or any similar system that provides locally and metrically accurate vehicle pose estimates.

IV. Method

Our calibration method comprises three steps. The first step involves extrinsic calibration of multiple LiDAR sensors to $\underrightarrow{\mathcal{F}}_V$. In the second step, we build a 3D map of the environment by transforming the LiDAR scans into $\underrightarrow{\mathcal{F}}_W$ based on the extrinsic calibration parameters for the LiDAR sensor and known vehicle poses. In the third and final step, we calibrate each radar sensor to the vehicle reference frame by finding the radar sensor pose with respect to $\underrightarrow{\mathcal{F}}_V$ and which minimizes point-to-plane distances between the radar scans and the 3D map and radial velocity errors between the measured and expected radial velocities assuming that the environment is static. We assume that known vehicle poses $\mathbf{T}_{WV}$ are provided by a GNSS/INS system or a similar system that provides locally and metrically accurate poses, i.e. LiDAR/visual odometry and a IMU-wheel-odometry system.

A. Extrinsic Calibration of Multiple LiDARs

We take a two-step approach to extrinsic calibration of multiple LiDAR sensors. The first step is extrinsic calibration of a single LiDAR sensor which entails estimation of the sensor's 6-DoF pose with respect to $\underrightarrow{\mathcal{F}}_V$. As this single-LiDAR calibration does not take other LiDAR sensors into account, the estimated sensor poses from individual calibration of multiple LiDAR sensors may not necessarily lead to pairwise geometric consistency between scans from different LiDAR sensors. This issue necessitates the additional and second step of refining the sensor poses such that we enforce

geometric consistency between scans from different LiDAR sensors.

1) Extrinsic Calibration of a Single LiDAR: Our single-LiDAR calibration approach is based on that of Levinson and Thrun [10]. To speed up the calibration by leveraging seed calibration parameter values, instead of performing alternating grid search over translation and rotation parameters, we employ non-linear least-squares optimization. We find the sensor's 6-DoF pose $\mathbf{T}_{VS}$ that minimizes the following cost function:

$$\sum_{b_i=1}^{B} \sum_{b_j=b_i-N}^{b_i+N} \sum_{k} w_k \rho((_W\mathbf{n}_k \cdot (_W\mathbf{p}_k - _W\mathbf{m}_k))^2) \quad (1)$$

where

$$_W\mathbf{p}_k = \mathbf{T}_{WV}\, \mathbf{T}_{VS}\, _S\mathbf{p}_k. \quad (2)$$

B is the number of beams in the LiDAR sensor, N is the number of neighboring beams we align each beam to, k iterates over the points observed by beam b_j, and $_W\mathbf{p}_k$ is the 3D world coordinates of the kth point observed by beam b_j and transformed into $\underrightarrow{\mathcal{F}}_W$ via $\mathbf{T}_{WV}$ and $\mathbf{T}_{VS}$. We find the n points from the neighboring beams and closest to $\mathbf{p}_k$, and fit a plane to the n points such that $_W\mathbf{n}_k$ is the unit normal of the plane in the world reference frame and $_W\mathbf{m}_k$ is the 3D world coordinates of the point belonging to the set of n points and closest to $_W\mathbf{p}_k$. ρ is a robust loss function that reduces the influence of outliers, and $w_k = 1$ if $\|_W\mathbf{p}_k - _W\mathbf{m}_k\| < d_{max}$ or $w_k = 0$ otherwise. In our implementation, we use $d_{max} = 1$.

2) Refinement: The previous step yields the pose of each LiDAR sensor with respect to $\underrightarrow{\mathcal{F}}_V$. Keeping the pose of the first LiDAR sensor fixed, we refine the pose of every other LiDAR sensor by minimizing the following cost function:

$$\sum_{i} w_i \rho((_W\mathbf{n}_i \cdot (_W\mathbf{p}_i - _W\mathbf{m}_i))^2). \quad (3)$$

i iterates over the points observed by the LiDAR sensor, and $_W\mathbf{p}_i$ is the 3D world coordinates of the ith point observed by the LiDAR sensor. We find the n points from the first LiDAR sensor and closest to $_W\mathbf{p}_i$, and fit a plane to the n points with $_W\mathbf{n}_i$ and $_W\mathbf{m}_i$ as the plane parameters.

B. Extrinsic Calibration of Multiple Radars

After obtaining the calibration parameters from extrinsic multi-LiDAR calibration, we build a 3D map of the environment by accumulating LiDAR scans from all calibrated LiDAR sensors. We leverage this map for extrinsic calibration of multiple radar sensors by finding the radar sensor poses that register the radar scans to the map as closely as possible. Given that the map is locally and metrically consistent, we can simplify the extrinsic multi-radar calibration problem to an extrinsic single-radar calibration problem which we solve for each radar sensor.

A radar scan corresponds to a set of point measurements $z_1, ..., z_N$ where $z = [r\ \theta\ \phi\ v_r]^T$ and r, θ, ϕ and v_r are the range, azimuth, elevation, and radial velocity respectively of the point. We obtain the 3D coordinates $\mathbf{p}$ of a point measurement:

$$\mathbf{p} = \begin{bmatrix} x \\ y \\ z \end{bmatrix} = \mathbf{f}\left(\begin{bmatrix} r \\ \theta \\ \phi \end{bmatrix}\right) = \begin{bmatrix} r\cos\theta\cos\phi \\ r\sin\theta\cos\phi \\ r\sin\phi \end{bmatrix} \quad (4)$$

Given the measurement covariance matrix $\mathbf{C_z}$:

$$\mathbf{C_z} = \begin{bmatrix} \sigma_r^2 & 0 & 0 \\ 0 & \sigma_\theta^2 & 0 \\ 0 & 0 & \sigma_\phi^2 \end{bmatrix}, \quad (5)$$

we obtain the covariance matrix $\mathbf{C_p}$ corresponding to $\mathbf{p}$:

$$\mathbf{C_p} = \mathbf{J_f} \mathbf{C_z} \mathbf{J_f}^T. \quad (6)$$

where $\mathbf{J_f}$ is the Jacobian of the function $\mathbf{f}$ from Equation 4. Given the known linear velocity $\mathbf{v}_{WV}$ of the vehicle in $\underrightarrow{\mathcal{F}}_W$, we obtain the linear velocity $\mathbf{v}_{SS}$ of the radar sensor in $\underrightarrow{\mathcal{F}}_S$:

$$\mathbf{v}_{SS} = \mathbf{R}_{SV}(\mathbf{R}_{VW}\, \mathbf{v}_{WV} + \omega_V \times \mathbf{t}_{VS}) \quad (7)$$

where ω_V is the angular velocity of the vehicle. Assuming that the environment is static, the linear velocity of a point measurement with respect to $\underrightarrow{\mathcal{F}}_S$ is equal to $-\mathbf{v}_{SS}$.

For each radar sensor, we find the 6-DoF pose of the sensor with respect to $\underrightarrow{\mathcal{F}}_V$ by minimizing the following cost function which is the sum of squared weighted point-to-plane distance residuals and squared weighted radial velocity residuals:

$$\sum_i (w_i \rho(w_{d_i} {d_i}^2) + \rho(w_{e_i} {e_i}^2)) \quad (8)$$

where

$$d_i = _W\mathbf{n}_i \cdot (_W\mathbf{p}_i - _W\mathbf{m}_i) \quad (9)$$

$$w_{d_i} = \frac{1}{_W\mathbf{n}_i^T \mathbf{C}_{\mathbf{p}_i}\, _W\mathbf{n}_i} \quad (10)$$

$$e_i = v_i + \mathbf{v}_{SS} \cdot \begin{bmatrix} \cos\theta\cos\phi \\ \sin\theta\cos\phi \\ \sin\phi \end{bmatrix} \quad (11)$$

$$w_{e_i} = \frac{1}{\sigma_{v_i}^2} \quad (12)$$

i iterates over the point measurements observed by the radar sensor. d_i is the point-to-plane residual, $_W\mathbf{p}_i$ is the 3D world coordinates of the ith point observed by the radar sensor, and $_W\mathbf{n}_i$ and $_W\mathbf{m}_i$ are the parameters of the plane fitted to the n points from the LiDAR map and closest to $\mathbf{p}_i$. w_{d_i} is the inverse of the projection of $\mathbf{C_p}$ onto the line with direction vector $_W\mathbf{n}_i$. e_i is the radial velocity residual, v_i is the measured radial velocity corresponding to point measurement i, and w_{e_i} is the inverse of the variance of the measured radial velocity. We obtain the standard deviation σ_{v_i} of the measured radial velocity from the radar sensor's published specifications [11]. The point-to-plane distance residuals based on position measurements from radar enforce the constraint that the point measurements are aligned with the LiDAR map, and the radial velocity residuals based on radial velocity measurements radar enforce the constraint that

the point measurements are stationary in $\underrightarrow{\mathcal{F}}_W$. The use of both residual types allows us to fully utilize all elements of the point measurement vector for extrinsic calibration. The robust loss function ρ reduces the influence of outliers that may result partly from moving objects in the environment. All non-linear least-squares optimizations described in this section are implemented using the Ceres Solver library [12].

V. EXPERIMENTS AND RESULTS

A. Experimental Setup

We use the Isuzu D-Max vehicle platform for our experiments and which is shown in Fig. 1. A dual-antenna GNSS/INS system with a tactical-grade IMU is installed in the vehicle, and provides state measurements at 200 Hz. We designate the reference frame of the GNSS/INS system as $\underrightarrow{\mathcal{F}}_V$. Four Velodyne HDL-32E LiDAR sensors are situated on the four corners of the roof rack, and each 3D LiDAR sensor yields a 360° scan with 2 cm range accuracy at 10 Hz. Four smartmicro UMRR-8F T146 radar sensors are installed in an all-surround configuration: two behind the front bumper, and two on the rear bumper. Each radar sensor provides a scan containing up to 255 points at 20 Hz; from the product datasheet [11], the range accuracy is the larger of 0.15 m and 1% of the measured range, the azimuth accuracy is 1°, and the elevation accuracy is 2°. For maximum calibration accuracy, the radar sensors are set to short-range mode which yields the highest range accuracy and limits the maximum range to 20 m. Otherwise, we set the radar sensors to long-range mode in everyday operating conditions. Given that our calibration method depends on features in the environment, to ensure calibration accuracy, each radar sensor should cumulatively observe a sufficient number of objects over the period during which the calibration data is collected. All sensor data is hardware-timestamped to sub-microsecond precision; such accurate time synchronization is made possible through the use of a time server.

To show that our extrinsic calibration method does not require overlapping fields of view between LiDAR and radar sensors, we only use the front two LiDAR sensors on the vehicle in our experiments. The front two radar sensors have wide overlapping fields of view with the front two LiDAR sensors. In contrast, the rear two radar sensors have minimal overlapping fields of view with the front two LiDAR sensors, and also, the front two radar sensors. Target-based methods for extrinsic calibration [6, 7] require a wide overlapping field of view between a LiDAR sensor and a radar sensor, and thus, cannot be easily performed for the sensor pair of a front LiDAR sensor and a rear radar sensor due to the minimal overlapping field of view.

For extrinsic multi-LiDAR calibration, data from the GNSS/INS system and the front two LiDAR sensors was recorded over a 100-meter run in an outdoor parking lot. To ensure that the 6-DoF pose of each LiDAR with respect to $\underrightarrow{\mathcal{F}}_V$ was fully observable, the vehicle was driven in constantly changing directions and driven over a curb that induced changes in the vehicle's roll or pitch. If the vehicle moves in a straight line, the x and y components of the position of the LiDAR sensor with respect to $\underrightarrow{\mathcal{F}}_V$ is not observable. Similarly, if the vehicle moves on a flat plane, the height of the LiDAR sensor with respect to $\underrightarrow{\mathcal{F}}_V$ is not observable. For extrinsic multi-RADAR calibration and repeatability analysis, data from the GNSS/INS system, the two front LiDAR sensors, and all radar sensors was recorded over ten 100-meter runs over a L-shaped trajectory in the same outdoor parking lot.

Fig. 1. The vehicle platform. Four 3D LiDAR sensors are mounted on the roof rack. Red circles mark the locations of a radar located behind the front bumper and two radars mounted on the rear bumper.

B. Calibration Results

We run the extrinsic multi-LiDAR calibration, and with the inferred calibration parameters corresponding to the 6-DoF pose of each LiDAR sensor with respect to the vehicle reference frame, we build a 3D map of the outdoor parking lot by transforming each scan from each LiDAR sensor into the world reference frame and accumulating all scans. Fig. 2 shows the resulting 3D map of the outdoor parking lot. The point cloud map appears crisp visually with no signs of smearing, indicating the high accuracy of the calibration parameters.

For each of the ten runs, we built a LiDAR map of the outdoor parking lot, and used the LiDAR map to perform extrinsic multi-radar calibration. From the ten runs, we obtained ten sets of calibration parameters corresponding to the 6-DoF pose of each radar sensor with respect to the vehicle reference frame.

The mean and standard deviation of each calibration parameter is recorded in Table I. Fig. 3 visualizes the mean position and orientation of each radar sensor with respect to $\underrightarrow{\mathcal{F}}_V$. The low standard deviations of the calibration parameters show that our calibration method produces accurate and highly repeatable results. The observation that the y and z components of the translation and rotation parameters have larger standard deviations than the x component can be attributed to the fact that the elevation measurement accuracy is 2 times worse than the azimuth measurement accuracy for the radar sensors. From comparing the mean of each calibration parameter with the seed value, we observe that

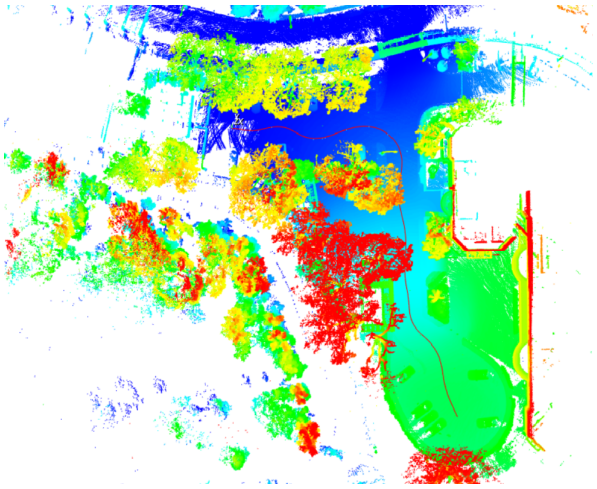

Fig. 2. A 3D map of the outdoor parking lot and built using the front two 3D LiDAR sensors on the vehicle. Map points are colored from blue to red in order of increasing height. A red line marks the vehicle's trajectory during the data collection process.

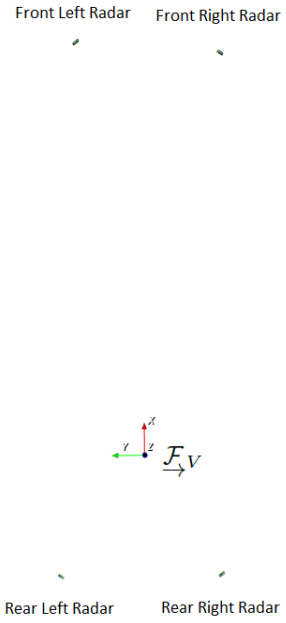

Fig. 3. A visualization of the mean position and orientation of each radar sensor with respect to the vehicle frame and as computed from our calibration method.

although seed translation and rotation parameters may differ by up to 1.8 m and 10° respectively from the final values, our calibration method is able to converge all the time, indicating a large convergence basin. The box plots shown in Fig. 4 show the spread of the calibration parameters. To facilitate ease of comparison, each calibration parameter has its mean subtracted away.

We perform an ablation experiment to determine the contributions of the point-to-plane distance residuals and the radial velocity residuals to the calibration accuracy and repeatability. For extrinsic multi-radar calibration, we minimize the following three different cost functions:

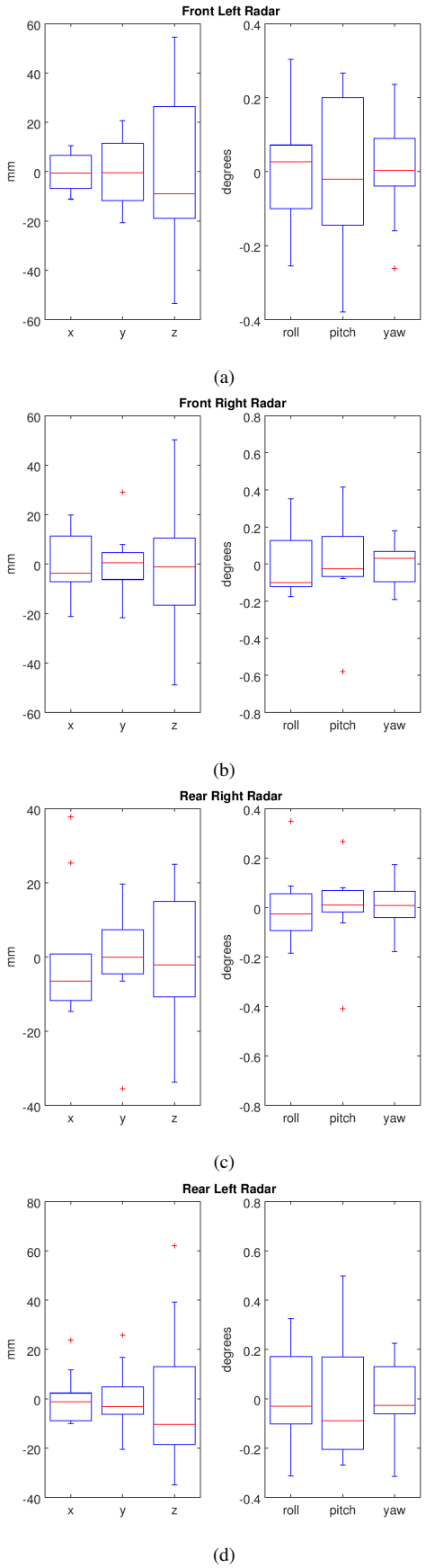

Fig. 4. Box plot of each extrinsic calibration parameter about its mean for 10 different calibration runs.

	Front Left Radar			Front Right Radar			Rear Left Radar			Rear Right Radar		
	Seed	Mean	Std Dev	Seed	Mean	Std Dev	Seed	Mean	Std Dev	Seed	Mean	Std Dev
x (m)	2	3.742	0.008	2	3.695	0.013	0	-1.087	0.011	0	-1.082	0.018
y (m)	0	0.607	0.014	0	-0.712	0.013	0	0.759	0.013	0	-0.689	0.015
z (m)	0	0.440	0.034	0	0.280	0.028	0	0.156	0.031	0	0.240	0.019
roll (°)	0	1.931	0.161	0	-0.216	0.183	0	-0.400	0.224	0	2.357	0.151
pitch (°)	0	-3.989	0.214	0	-2.851	0.259	0	-0.609	0.272	0	1.055	0.169
yaw (°)	45	37.829	0.141	-45	-37.006	0.122	135	142.637	0.158	-135	-146.391	0.110

TABLE I

EXTRINSIC CALIBRATION PARAMETERS FOR EACH OF THE FOUR RADAR SENSORS ON THE VEHICLE. THE MEANS AND STANDARD DEVIATIONS ARE DERIVED FROM TEN RUNS.

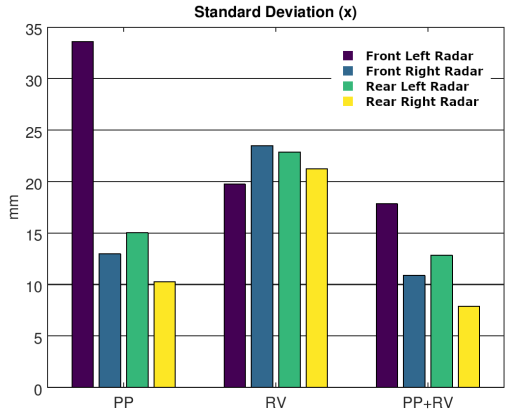

Fig. 5. PP: Minimization of point-to-plane distance residuals. RV: Minimization of radial velocity residuals. PP+RV: Minimization of both point-to-plane distance and radial velocity residuals.

1) $J_{PP} = \sum_i w_i \rho(\mathbf{d}_i^T \mathbf{D}_i \mathbf{d}_i)$
2) $J_{RV} = \sum_i \rho(e_i^T E_i e_i)$
3) $J_{PP+RV} = \sum_i (w_i \rho(\mathbf{d}_i^T \mathbf{D}_i \mathbf{d}_i) + \rho(e_i^T E_i e_i))$

J_{PP} only contains point-to-plane distance residuals, J_{RV} only contains radial velocity residuals, and J_{PP+RV} contains both types of residuals. Fig. 5 shows the standard deviation of the x-translation component of the calibration parameters for each cost function. From the figure, we observe that using both types of residuals gives the lowest standard deviation. This observation shows that utilizing all properties of radar measurements enables us to maximize calibration accuracy and repeatability.

To facilitate a qualitative analysis of the calibration accuracy, we show the point cloud maps built by accumulating scans from all four radar sensors on the vehicle, and with seed and optimized calibration parameters. Fig. 6 shows the point cloud map based on seed calibration parameters, and Fig. 7 shows the point cloud map based on the optimized calibration parameters. The visually sharp outlines of the parked cars in the point cloud map corresponding to the optimized calibration parameters point to the high accuracy of our calibration method. We show a scan from the front left radar sensor interposed against the LiDAR map in Fig. 8. From visual inspection, the scan is aligned well with the LiDAR map due to the accurate calibration parameters estimated by our extrinsic calibration method.

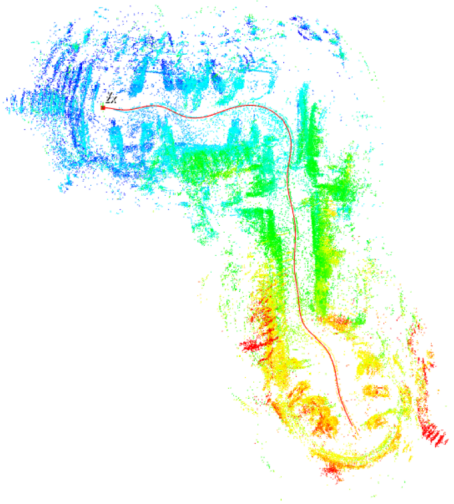

Fig. 6. A 3D map from accumulated radar scans with seed calibration parameters. There is significant smear across the entire map, and parked cars cannot be clearly seen.

Fig. 7. A 3D map from accumulated radar scans with estimated calibration parameters. The outlines of parked cars can be clearly seen.

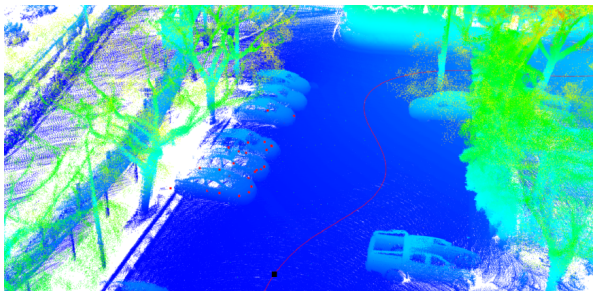

Fig. 8. A radar scan from the front left radar superimposed against the 3D LiDAR map. Red points denote the radar scan while a black square on the vehicle's trajectory represented as a red line marks the vehicle's position corresponding to the time of the radar scan.

VI. CONCLUSIONS

Through real-world experiments, we have demonstrated our extrinsic calibration method for multiple LiDAR and radar sensors to be highly accurate and repeatable. To the best of our knowledge, our method is the first published method for automatic targetless calibration of multiple LiDAR and radar sensors. The automatic and targetless nature of our calibration method allows a vehicle equipped with LiDAR and radar sensors to be easily calibrated anywhere and anytime without the need for a calibration target and human intervention. In addition, our calibration method does not require overlapping fields of view between LiDAR and radar sensors. Future work will focus on all-weather localization and perception with calibrated radar sensors.

REFERENCES

[1] Jianhao Jiao, Yang Yu, Qinghai Liao, Haoyang Ye, and Ming Liu. Automatic calibration of multiple 3d lidars in urban environments. In *IEEE/RSJ International Conference on Intelligent Robots and Systems (IROS)*, 2019.

[2] W. Maddern, A. Harrison, and P. Newman. Lost in translation (and rotation): Rapid extrinsic calibration for 2d and 3d lidars. In *IEEE International Conference on Robotics and Automation (ICRA)*, 2012.

[3] Lionel Heng, Benjamin Choi, Zhaopeng Cui, Marcel Geppert, Sixing Hu, Benson Kuan, Peidong Liu, Rang Nguyen, Ye Chuan Yeo, Andreas Geiger, Gim Hee Lee, Marc Pollefeys, and Torsten Sattler. Project autovision: Localization and 3d scene perception for an autonomous vehicle with a multi-camera system. In *IEEE International Conference on Robotics and Automation (ICRA)*, 2019.

[4] Gaurav Pandey, James R. McBride, Silvio Savarese, and Ryan M. Eustice. Automatic extrinsic calibration of vision and lidar by maximizing mutual information. *Journal of Field Robotics (JFR)*, 32(5):696–722, 2015.

[5] C. Schöller, M. Schnettler, A. Krämmer, G. Hinz, M. Bakovic, M. Güzet, and A. Knoll. Targetless rotational auto-calibration of radar and camera for intelligent transportation systems. In *IEEE Intelligent Transportation Systems Conference (ITSC)*, 2019.

[6] J. Peršić, I. Marković, and I. Petrović. Extrinsic 6dof calibration of 3d lidar and radar. In *European Conference on Mobile Robots (ECMR)*, 2017.

[7] J. Domhof, K. Julian F. P., and K. Dariu M. An extrinsic calibration tool for radar, camera and lidar. In *IEEE International Conference on Robotics and Automation (ICRA)*, 2019.

[8] R. Izquierdo, I. Parra, D. Fernández-Llorca, and M. A. Sotelo. Multi-radar self-calibration method using high-definition digital maps for autonomous driving. In *IEEE International Conference on Intelligent Transportation Systems (ITSC)*, 2018.

[9] D. Kellner, M. Barjenbruch, K. Dietmayer, J. Klappstein, and J. Dickmann. Joint radar alignment and odometry calibration. In *International Conference on Information Fusion (FUSION)*, 2015.

[10] J. Levinson and S. Thrun. Unsupervised calibration for multi-beam lasers. In *International Symposium on Experimental Robotics (ISER)*, 2010.

[11] smartmicro umrr-8f t146 data sheet. `http://www.smartmicro.de/fileadmin/user_upload/Documents/Automotive/UMRR_Automotive_Type_146_Data_Sheet.pdf`.

[12] Sameer Agarwal, Keir Mierle, and Others. Ceres solver. `http://ceres-solver.org`.